Sonoluminescence: The hydrodynamical/chemical approach: A detailed comparison to experiment

Michael P. Brenner [1], Sascha Hilgenfeldt [2], and Detlef Lohse [2]

[1] *Department of Mathematics, Massachusetts Institute of Technology, Cambridge, MA 02146, USA*

[2] *Fachbereich Physik der Universität Marburg, Renthof 6, 35032 Marburg, Germany*

(August 6, 1997)

Detailed comparison between experimental data and the recent hydrodynamical/chemical approach towards single bubble sonoluminescence (SBSL) is offered. Many of the unknowns can be resolved following this approach.

Keywords: Single bubble sonoluminescence / bubble dynamics / shape oscillations / rectified diffusion / relevance of inert gases and molecular gas dissociation hypothesis for sonoluminescence/ SBSL bubbles as high temperature chemical reaction chambers

I. INTRODUCTION

The unknowns of single bubble sonoluminescence (SBSL [1, 2]) have been defined by Putterman's UCLA group in Ref. [2]. This proceedings contribution argues that many of the unknowns can be rationally resolved through a combination of classical bubble dynamics [3–13] supplemented by a consideration of chemical effects [14–16]. Through detailed comparisons between experiments and the classical bubble dynamics/ chemical theory, the following problems of reference [2] are adequately resolved:

- What determines the radius of the SBSL bubble?
- What determines the upper and lower sound pressure thresholds above which one can observe SL?
- Why are noble gases so essential for producing stable, bright bubbles?
- Why do pure diatomic gas bubbles jitter and give such dim light?

Other questions remain open, in particular

- What exactly is the light emitting mechanism?

Some of the questions posed in Ref. [2] can eventually only be answered by experiment, e.g., whether one can measure the spectrum of SL beyond the ultraviolett cutoff of water.

The goal of this proceedings contribution is to give further detailed comparisons between experimental measurements [1, 2, 17–20] and the hydrodynamic/chemical approach, in addition to the comparisons already made in Refs. [11, 14–16].

The organization of the paper is as follows: In section 2 we give a short review of the hydrodynamic/chemical approach towards SBSL [9, 11, 15], focusing on the conditions necessary for SBSL to occur. The main part of the paper (section 3) offers a detailed comparison between theory and experiment. Section 4 presents conclusions and outlines the most important remaining open questions from our point of view.

II. THE HYDRODYNAMIC/CHEMICAL APPROACH TOWARDS SBSL

A. Experimental parameters

The important adjustable parameters in an SBSL experiment are the driving pressure amplitude P_a, the gas pressure overhead p_∞, and the chemical composition of the dissolved gas; to change the latter, the inert gas ratio ξ of the mixture is often varied. Further experimental parameters are the temperature of the liquid, its viscosity ν_l, and the surface tension σ; we will restrict ourselves to the values for water. – The driving frequency ω is fixed at the resonance frequency of the Crum cell.

The ambient radius R_0 of the bubble, i.e., the bubble radius at ambient conditions of $P_0 = 1\text{atm}$ and room temperature, is not an adjustable parameter but the system chooses R_0 dynamically. It can be measured by Mie scattering techniques [21], or by the "ringing down" technique of Holt and Gaitan [17].

B. Bubble hydrodynamics

The goal of the theory of bubble hydrodynamics is to delimit the regime of parameter space where stable sonoluminescence can occur. Since the parameter space is multi–dimensional (P_a, p_∞, ξ, and R_0), and the dynamics involves timescales spanning ten orders of magnitude (from the timescale of the light flash ($100 - 300ps$ [22] or even shorter [2, 23, 24]) to the diffusive timescale ($\sim 1s$)), it is necessary to make approximations in modeling the hydrodynamics of sonoluminescence.

Experiments [6] have demonstrated that the *Rayleigh-Plesset* (RP) approximation for the spherical bubble radius $R(t)$ [3, ?, 4, 13] accurately reproduces the bubble radius as a function of time in the parameter regime of sonoluminescence. The pressure

$p(R,t)$ inside the bubble is assumed to have no spatial variations; the temporal variation of the pressure follows from a van der Waals polytropic law with a polytropic exponent γ. The Rayleigh-Plesset ODE reads

$$R\ddot{R} + \frac{3}{2}\dot{R}^2 = \frac{1}{\rho_l}\left(p(R,t) - P(t) - P_0\right) + \frac{R}{\rho_l c_l}\frac{d}{dt}\left(p(R,t) - P(t)\right) - 4\nu_l\frac{\dot{R}}{R} - \frac{2\sigma}{\rho_l R} \quad (1)$$

Here, $P(t) = P_a \cos\omega t$ is the acoustic driving field with period $T = 2\pi/\omega \approx 38\mu s$, and ρ_l and c_l are the density and speed of sound of water, respectively. The polytropic law not only gives the pressure in the bubble but also the temperature in this approximation. References [15, 16] follow Plesset and Prosperetti [4] and introduce a time dependent Peclet number, giving a time dependent polytropic exponent $\gamma(t)$. For all times but the bubble collapse $\gamma = 1$, i.e., isothermal bubble motion. At the bubble collapse $\gamma = 5/3$ for argon and $\gamma = 7/5$ for nitrogen. The approximation gives temperatures as high as 10^5K at the bubble collapse, see [16]. The actual temperature values are probably even higher thanks to gas motion (i.e. shock wave formation [25, 26]), but the general features of our results presented here are robust towards such changes in the model.

We call the approach of using a simplified model of bubble dynamics to understand sonoluminescing bubbles the *RP-SL-bubble approach* [11]. The advantage of this approach is that it is possible to explore the entire SL parameter space and compute phase diagrams. The disadvantage is that we cannot make any statement on the gas dynamics in the bubble and how exactly the light is emitted. We will demonstrate below that the predictions of the RP-SL bubble approach agree (within experimental error) with experiments, and therefore provide adequate explanations to the unknowns listed above.

C. Conditions for SL

We now formulate the necessary conditions for SL, within the RP-SL bubble approach. Four conditions are necessary for stable SBSL [9, 11, 15]: 1. Energy focusing, 2. Shape stability, 3. Diffusive stability, and 4. Chemical stability.

Energy focusing: The essential condition for SBSL is sufficient *energy transfer* from the fluid to the gas bubble and focusing of the energy. We take as a criterion for energy transfer and the resulting heating of the gas that the Mach number of the bubble wall (with respect to the speed of sound in the gas) has to be larger than one ($|M_{gas}| = |\dot{R}|/c_{gas} \gtrsim 1$). From RP simulation, it is easy to compute a corresponding line in the $P_a - R_0$ parameter space (dashed in Fig. 1). This criterion marks the onset of SL both within conventional shock theories [25, 26] and within the acoustic resonator theory [27].

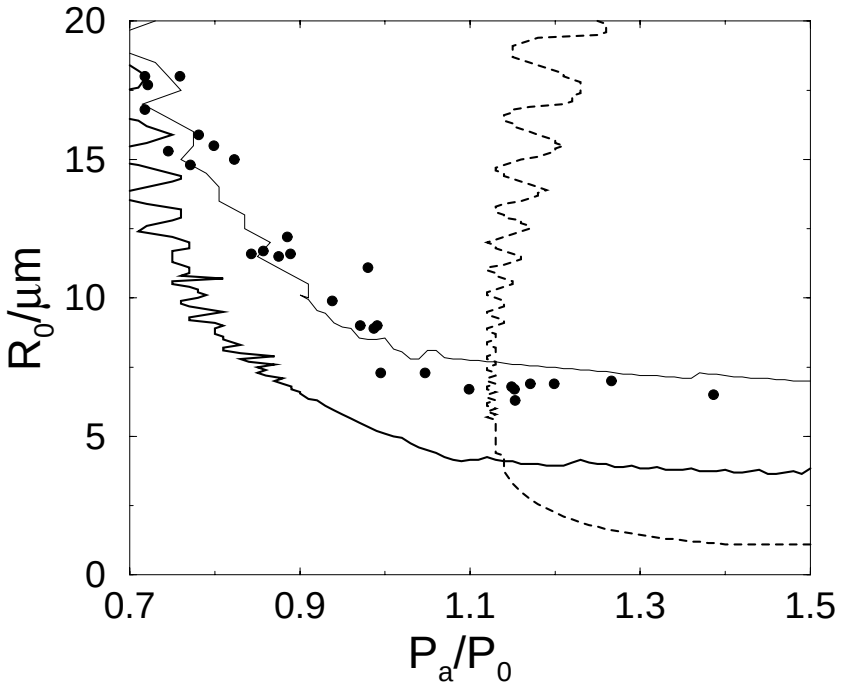

FIG. 1. Stability conditions for a bubble in the $P_a - R_0$ parameter space. Bubbles above the line $M = 1$ (dotted) fulfill the energy focusing condition. Bubbles below the shape instability lines (solid thick line) are stable towards non-spherical parametric surface oscillations (for the SL region, $n = 2$ is the most unstable mode). These curves are for water, $\nu_l = \nu_{water}$. The figure also contains the data for the shape instability line as measured by Holt and Gaitan [17] (circles). One can obtain more stable bubbles by changing the parameters of the equations. For illustrative purposes, we include here a calculation where we assume a larger (unphysical) viscosity, as done in Barber et al. [2]. The solid thin line shows the shape stability border for a viscosity $\nu_l = 4\nu_{water}$ – the $M_{gas} = 1$ curve hardly changes in this case. Both experiment and theory refer to a frequency $\omega/2\pi = 20.6$kHz. Not shown in the figure is the (short time scale) Rayleigh-Taylor shape instability [9, 11] which sets in around $P_a = 1.4 - 1.5$atm and presumably gives the upper threshold of the SL domain.

Shape stability: In order to emit light for a large number of driving cycles, the bubble should be (spherically) *shape stable* to guarantee sufficient focusing power of the collapse and to avoid bubble disruption and fragmentation. The idea of the RP approximation can be extended to deal with *shape oscillations* [9, 11, 28]. In a linear approximation around the spherically symmetric solution $R(t)$ one obtains an ODE for the amplitude $a_n(t)$ of a spherical harmonic distortion of order n. To deal with nonlocal effects, we introduced a boundary layer approximation of the vorticity field around the bubble. It turns out that different types of shape stabilities exist, operating on different time scales [9, 11]. Our results – shown in Fig. 1 – quantitatively

depend on the details of the approximation (e.g., the exact thickness of the boundary layer), however, the qualitative features and the rough magnitude of the results do not. Together with the energy focusing criterion, the shape stability lines define a small region in $P_a - R_0$ parameter space of potentially sonoluminescing bubbles (see Fig. 1).

Diffusive stability: *Diffusive processes* can also be understood within the RP approach to the SL bubble [7, 8, 10, 29]. At first sight this is surprising because there is no diffusive timescale in the RP equation. However, the boundary conditions from the full advection-diffusion problem are determined by the RP dynamics [30], as very nicely elaborated in the careful work of Fyrillas and Szeri [7] and Löfstedt et al. [8]. By separating the slow diffusive timescale from all timescales in the RP equation the diffusive equilibrium and its stability can be understood solely from the RP dynamics.

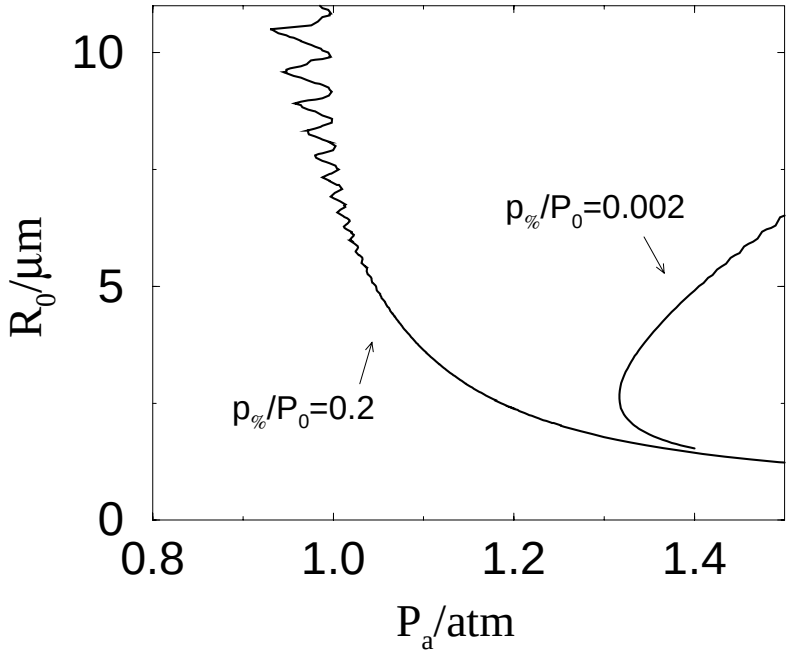

FIG. 2. Diffusive equilibria for $p_\infty/P_0 = 0.20$ and $p_\infty/P_0 = 0.002$ in the $P_a - R_0$ phase space. The dissolved gas is pure argon, $p_\infty = p_\infty^{Ar}$.

The calculations for pure argon as dissolved gas were done in Ref. [11] and yield the lines in Fig. 2, which give the location of diffusive equilibria in $P_a - R_0$ parameter space. Also, the stability of the equilibria can be immediately read off from these curves: points with positive slope are stable, those with negative slope unstable. For relatively large argon pressure p_∞^{Ar}/P_0 (e.g. 20%) the bubble behaves as follows: if the radius is below the equilibrium line, it shrinks and dissolves, whereas above the

line it grows by rectified diffusion, until shape instabilities cause mass loss (shedding of microbubbles) and limit the growth. We call this state, in case light is emitted, *unstable SL*.

For very small p_∞^{Ar}/P_0 (e.g. 0.2%) the situation is entirely different. The curve of diffusive equilibria bends back, displaying a branch of positive slope and thus *stable* equilibria. If this branch intersects the shaded region of figure 1, where the energy focusing condition and the shape stability condition are fulfilled, *stable SL* becomes possible. The light emitting bubbles have a defined R_0, which does not change by diffusion. These bubbles oscillate in precisely the same way in every cycle, keeping fixed phase and intensity of light emission for *ever*. From a practical point of view, the sealing of the Crum cell (as influx of air has to be avoided) sets limitations.

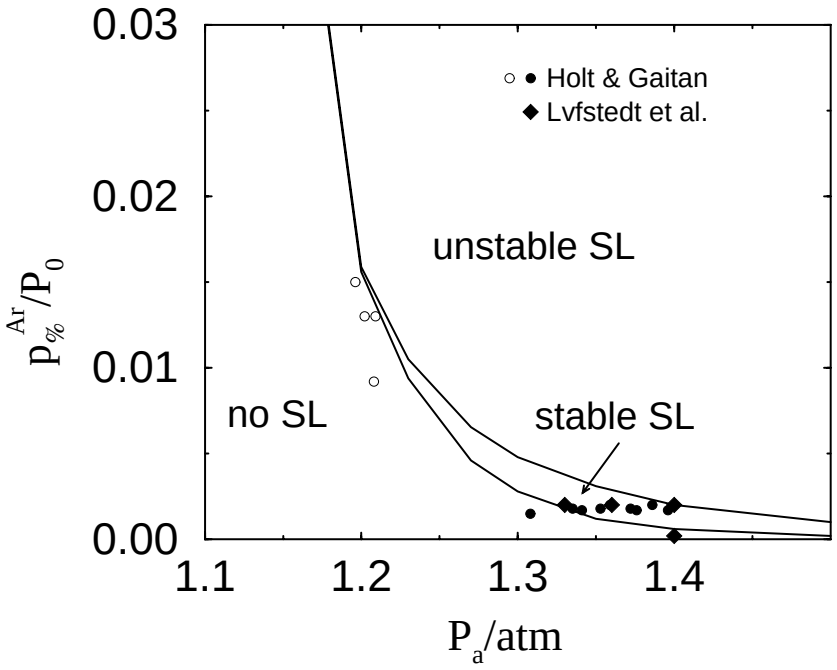

FIG. 3. Phase diagram for pure argon bubbles in the p_∞^{Ar}/P_0 versus P_a/P_0 parameter space. Stable SL is only possible in a very small window of argon concentration. The experimental data points included for comparison refer to observed stable SL (filled symbols) or stable non-SL bubbles (open symbols) from Refs. [8] (diamonds) and [17] (circles) and show good agreement with the theory. Note that only those data can be included for which P_a, p_∞ and ξ are experimentally known.

From an experimental point of view the problem with phase diagrams such as Fig. 1 or 2 is that R_0 is not freely adjustable (cf. Section II A). Therefore, we in addition give the phase diagram [11, 15] Fig. 3 in the $P_a - p_\infty^{Ar}$ phase space of the directly controllable experimental parameters, obtained through evaluation of diffusive stabi-

lity curves for many overhead pressures p_∞^{Ar}/P_0. We restrict ourselves to argon (or any other inert gas) here; the extension to diatomic gas mixtures is straightforward [14–16], as we will see in the next subsection. For given P_a and p_∞^{Ar} we predict with Fig. 3 whether the bubble is in the diffusively unstable SL state, the diffusively stable SL state, or does not show SL at all. We stress that the theory relies only on classical formulations of bubble dynamics, and requires *no* fit parameters.

Chemical stability: The reason that *chemical instabilities* (i.e., dissociation and subsequent reactions) have to be considered [14–16] is that the high central bubble temperatures of at least several 10^4 K are more than sufficient to dissociate any molecular gas constituent, including N_2 and O_2 in the case of an air-filled bubble. The formed radicals immediately react with water molecules to a variety of products, probably predominantly NO, NH, and NO_2. These substances are extremely soluble in water and are readily absorbed by the surrounding liquid, leaving only the inert gas component of air (i.e., argon) inside the bubble.

To model this mechanism within the RP-SL bubble approach, we have to assume an equation of state for the gas in the bubble and an Arrhenius type reaction law for molecular gases, as done in Refs. [15, 16]. Consider a mixture (at p_∞) of a molecular gas (say, nitrogen) and argon at a ratio of $\xi = 0.01$. As molecular gases dissociate at the high temperatures achieved in the SL bubble collapse and their reaction products subsequently dissolve in water, *only the partial argon pressure* $p_\infty^{Ar} = \xi p_\infty$ *is relevant for stability.* To put it in a nutshell, sonoluminescing "air" bubbles are in fact argon bubbles!

The chemical dissociation mechanism introduces new features into the P_a–R_0 phase diagram of Fig. 2. Consider an air bubble at a partial pressure of $p_\infty/P_0 = 20\%$. For low P_a, the (non-SL) bubble does not heat sufficiently for chemical reactions to occur. Thus, p_∞ is the relevant quantity for the diffusive stability – in this case, the bubble is diffusively unstable (curve A in Fig. 4a). For high P_a, the bubble contains only argon; thus, the relevant quantity is now the argon partial pressure $p_\infty^{Ar}/P_0 \approx 0.2\%$ – which allows for stable equilibria (curve C). Because of the topology of the diagram Fig. 4, another *stable* equilibrium line must necessarily exist in between. Indeed, such a curve (B) is found in our computations. These equilibria describe bubbles for which chemistry can only partially eliminate the reactive gases; they generally occur when the bubble wall is not supersonic, so there is no sonoluminescence.

Chemical reactions play a role as a *transient* phenomenon when slowly increasing the forcing amplitude – the bubble will be "cleaned" from its molecular gases. But chemistry is also important in the *stationary* state: When the bubble is big, the pressure inside is tiny and the dissolved gas mixture (N_2 and Ar) is sucked into the bubble. On collapse, the N_2 reacts and the reaction products are thrown out of the bubble and dissolve. The bubble can be understood as a micrometer size reaction chamber for high temperature chemistry, as we suggested in Ref. [15].

a)

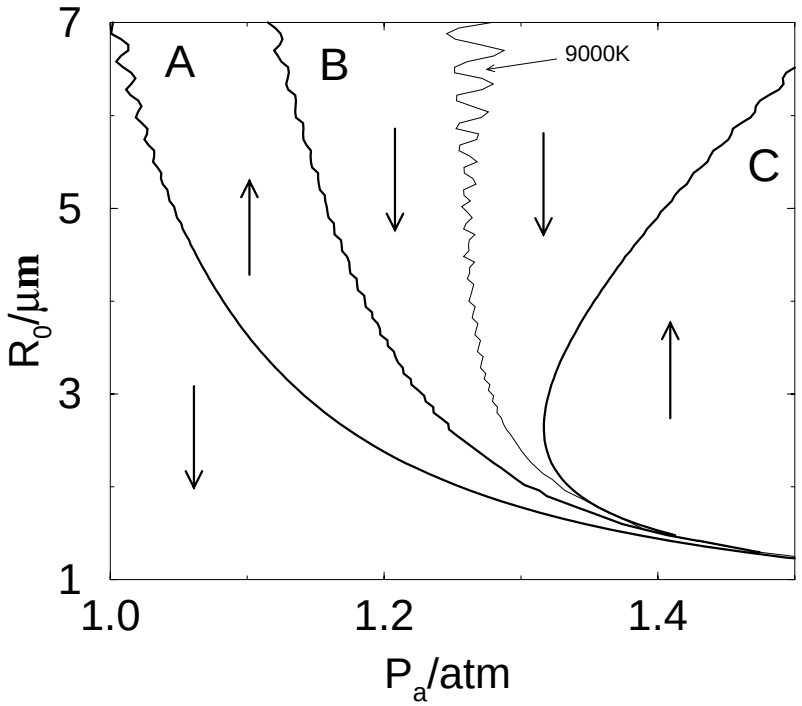

b)

FIG. 4. (a) Phase diagram for air (i.e. $\xi = 0.01$) at $p_\infty/P_0 = 0.20$ in the $P_a - R_0$ space. The arrows indicate whether the ambient radius grows or shrinks at this parameter value. Curve A denotes the expected *unstable* equilibrium for an air bubble at this high gas pressure, on curve C the bubble only contains argon. The intermediate curve B necessarily exists because of the topology of the diagram, and reprents an additional stable equilibrium. The thin curve shows when the nitrogen dissociation threshold $\sim 9000K$ is reached. (b) Experimental measurement of the same phase diagram by Holt and Gaitan (adapted from figure 1 of [17] with kind permission of the authors). Bubbles in shaded areas are shape stable.

III. COMPARISON TO EXPERIMENT

A. Stable vs. unstable SBSL

According to our above phase diagram Fig. 3 for argon as dissolved gas *stable SL* should only be possible for tiny gas pressures in the range of (for $P_a = 1.3$atm) $p_\infty^{Ar}/P_0 = 0.2 - 0.4\%$. Indeed, Barber et al. [2] observe stable SL at $p_\infty^{Ar} = 3$mmHg, corresponding to 0.4%.

At larger $p_\infty^{Ar} = 50$mmHg and $p_\infty^{Ar} = 200$mmHg (6% and 20% saturation, respectively) unstable SL is observed, again as expected from Fig. 3. This phase is characterized by an increase of the relative phase of light emission with respect to the driving pressure on the slow (diffusive) timescale $\sim 1s$, followed by a rapid breakdown and another subsequent increase. The light intensity itself behaves in the same way (cf. [2]) and the bubble is reported to be dancing or jiggling [1, 31]. This state of SL is also unstable in the sense that often all of a sudden the bubble disappears, i.e., it cannot be trapped in the acoustic field for a very long time. The same features of unstable SL can also be seen in the *acoustic* emission of the bubble [19].

In Ref. [12] we interpreted this behavior as a signature of bubble growth by rectified diffusion (see also the previous section). When growing, the bubble runs into the shape instability line of Fig. 1. Consequently, the bubble breaks up and microbubbles pinch off, leading to a recoil which makes the bubble dance. The (parameter free) theoretical calculations in Ref. [11] could produce results for the phase of light emission which resemble those of figure 27 of [2].

B. Only the argon partial pressure is relevant

For gas mixtures of nitrogen (or oxygen) and argon one expects the same two phases "stable SL" and "unstable SL", but at a $(1/\xi)$ times higher total gas concentration $p_\infty = p_\infty^{Ar}/\xi$. Moreover, according to the chemical hypothesis the type of reactive gas in the mixture is irrelevant for diffusive stability in the regime of large P_a. Indeed, as reported by Barber et al. [2], argon-oxygen mixtures and argon-nitrogen mixtures show very similar behavior, see figure 24 of this reference. Therefore, we put all available data for stable SL into the p_∞^{Ar} vs P_a phase diagram; very good agreement with our prediction is found. Also for unstable SL the relevant value $p_\infty^{Ar} = \xi p_\infty$ is always in the correct domain of Fig. 3.

In Fig. 5 we show Barber et al.'s experimental results for the SL intensity of argon-nitrogen mixtures. The largest intensity occurs for stable SL. Acording to the phase diagram Fig. 3 at $P_a = 1.3$atm SL is stable between $p_\infty^{Ar}/P_0 = 0.002 - 0.004$. This corresponds to $p_\infty/P_0 = 0.1 - 0.2$ for a N_2/Ar mixture with 1% argon (or also for air) and to $p_\infty/P_0 = 0.01 - 0.02$ for a N_2/Ar mixture with 10% Ar. Indeed, these are the pressure overheads where the corresponding SL intensities peak in Fig. 5.

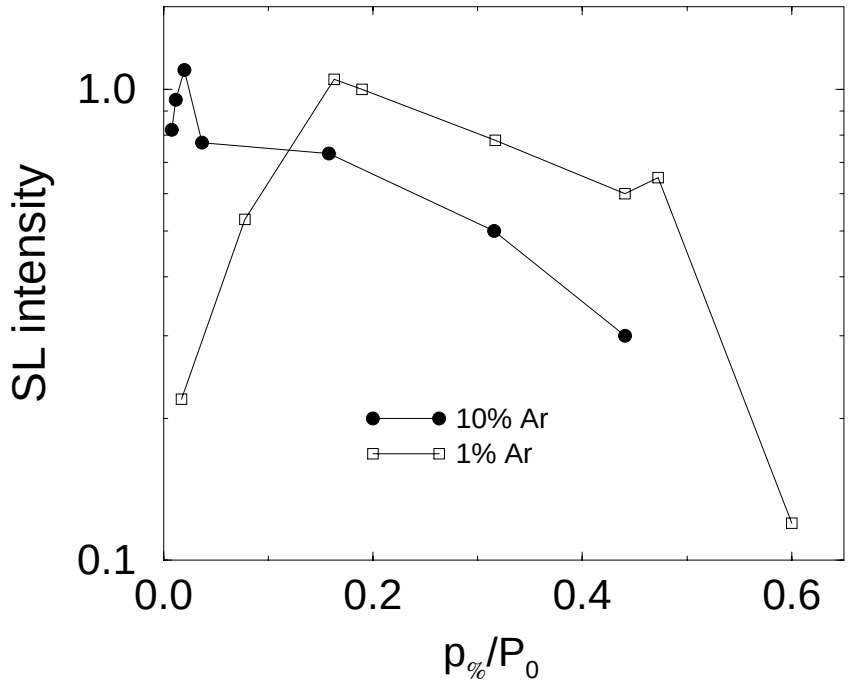

FIG. 5. SL intensity (normalized to air) from a SL bubble in water as a function of the gas mixture p_∞/P_0 for two different argon-nitrogen gas mixtures. The data are taken from figure 23 of Barber et al. [2].

C. Bubble reaction to forcing pressure changes

What happens when slowly increasing the forcing pressure P_a for fixed p_∞/P_0? The Putterman group has done various experiments of this kind and the results are given in the "waterfall plots" figs. 18, 21, 30, 32, 33, 42, 70 of Ref. [2]. All of these plots can be understood along the lines of the diffusive/chemical theory of Refs. [14–16]. Let us take a look at some of these results:

Pure argon: Consider e.g. the case of pure Ar dissolved at $p_\infty^{Ar}/P_0 = 0.004$, cf. [2]. According to Fig. 2, bubbles forced with $P_a < 1.2$atm dissolve. On increasing P_a beyond 1.2atm, the bubble follows the line of stable diffusive equilibria in Fig. 2 and its ambient size increases, also leading to a larger maximal radius, see figure 42 of [2]. Finally, it hits the shape instability (cf. Fig. 1) and gets destroyed.

Inert/reactive gas mixtures: For gas mixtures, say, a 1% xenon doped nitrogen bubble at $p_\infty/P_0 = 0.20$ or air bubble (cf. [2] for both cases), the sequence of events on increasing P_a can be read off Fig. 4. For low P_a the bubble is diffusively unstable and "dances". At a certain pressure around $P_a \sim 1.1$atm (see [16]) the bubble gets trapped by the stable equilibrium B and does not jiggle any more. On further increase of

P_a it decreases in size R_0 along curve B until it reaches the stable equilibrium C, now increasing its ambient size again. This sequence of events was reported already by Gaitan [1] and later again and again by various experimental groups, see e.g. Ref. [2].

Hysteresis for low inert gas content: If the partial pressure of inert gas is very low, say, $p_\infty/P_0 = 0.20$ and $\xi = 0.001$ as in figure 21 of Ref. [2] or the theoretical analogue figure 13 of Ref. [16], there is no stable SL around $P_a = 1.1\text{atm} - 1.3\text{atm}$. However, stable bubbles are still possible in this range, in analogy to those on curve B of Fig. 4a. These bubbles contain a slightly enhanced argon concentration. At $P_a = 1.4\text{atm}$ the stable equilibrium curve C is reached, displaying stable SL. As reported by Löfstedt et al. [8] and explained in detail in Ref. [16], this sequence of events shows hysteresis: Bubbles on branch C can be reached by slowly increasing P_a, but when decreasing P_a, the bubbles on branch B cannot be reestablished, because bubbles on branch C contain pure argon.

Hysteresis at the onset of SL: Another wonderful hysteresis experiment has recently been performed by Matula and Crum [18], now for unstable SL in air bubbles. Here, the bubble is boosted from the non-SL regime to the SL regime by a sudden increase of P_a (see also [2]). The radius adjusts within less than a second through rectified diffusion, whereas it takes several seconds for the chemical reaction to clear the bubble from N_2 and O_2. Finally, only argon remains and the bright signal of stable sonoluminescing bubbles is emitted. As seen from figure 35 of Ref. [2] the SL turn on time is in the range of seconds for air, whereas it takes only several 100 cycles for pure argon bubbles. Now Matula and Crum sweep down P_a below the SL threshold for some 2700 cycles. Diffusive processes are too slow to change the contents of the bubble (argon) abruptly. Therefore, if P_a is increased again after 2700 cycles, the bubble emits light immediately, which shows very nicely that argon has accumulated before.

D. Bubble size

We now come to a more quantitative comparison of bubble radii. The phase diagrams 2 and 4 predict the fixed bubble size of stable SL and with the help of Fig. 1 the range of possible bubble radii of unstable SL can also be given.

Holt and Gaitan [17] have measured the phase diagram Fig. 4b experimentally using air, and have identified both stable SL equilibria at the expected location for pure argon concentrations (curve C) and stable non-SL bubbles for smaller driving pressures (curve B). The agreement with our theory Fig. 4a is very good.

Figure 6 compares the experimental ambient radii given in [2] and the theoretical predictions following from the approach of Refs. [15, 16]. The curves show the same features. For low P_a there is unstable SL. The bubble grows from A up to the shape instability. The measured radii (circles) in this range have to be interpreted as either

instantaneous or averaged values from Mie scattering data. The small discrepancies could be a consequence of many factors, including: (a) the simplistic modeling assumptions made in our calculations (e.g. for the internal bubble temperature and for the chemical reactions) and (b) the experimental uncertainties in both P_a and R_0; the uncertainties in the latter are related to the unrealistic values of the fluid parameters (σ, ν_l, γ) assumed by Barber et al. [2] for determining R_0. – Also, the onset of light emission is well described with the RP–SL approach.

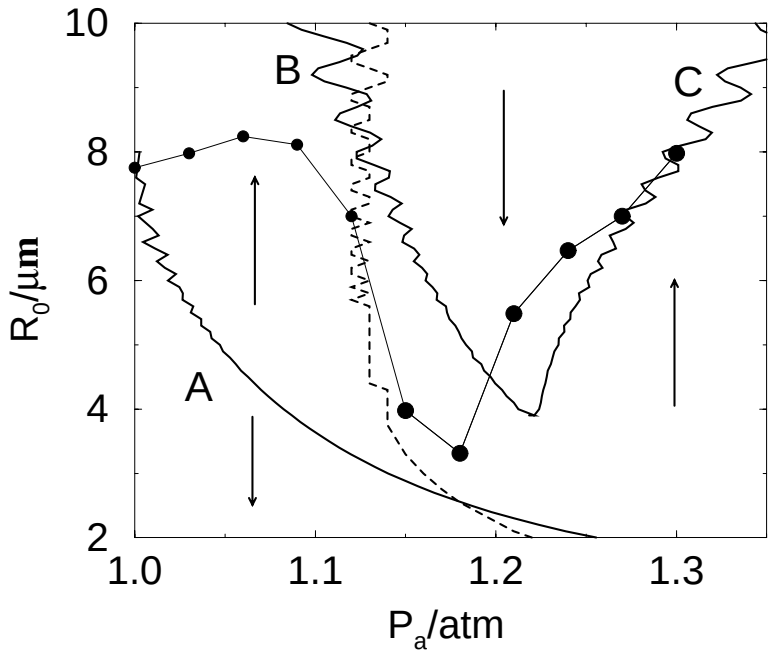

FIG. 6. Circles show the ambient radii R_0 for a 150mmHg ($p_\infty/P_0 = 20\%$) bubble of 5% argon in nitrogen as they follow from a 4 parameter fit to the RP equation to Mie scattering data performed in [2] (leading to unphysical values for σ, ν_l, and γ). Light emission from the bubble is indicated by larger circles. The data are taken from figure 43 of Ref. [2]. The first couple of data points represent unstable bubbles They grow by rectified diffusion up to the parametric shape instability which for clarity is not shown in this figure (but see figure 1). The solid lines result from our theory for the same frequency $\omega/2\pi = 23$kHz as employed in the experiment. B and C represent stable equilibria, A an unstable equilibrium. The thick dotted line is the $M_{gas} = 1$-curve corresponding to that of figure 1. Indeed, bubbles only grow to the right of this curve. Arrows illustrate regions of growing and shrinking bubbles.

E. Shape stability thresholds

In our theoretical Fig. 1 we included the experimental data measured by Holt and Gaitan (priv. comm. and Ref. [17]). The two curves show the same features, although the measured values of the upper domain of stability are slightly larger than our theoretical value. One of the reasons presumably is that there is some freedom in the boundary layer approximation done in Refs. [9, 11]. Of course, by changing details of that approximation it is possible to achieve a better quantitative description. For example, by taking a value for the liquid viscosity which is four times as large as that of water (the value Barber et al. take for their fits in Ref. [2]) the calculated domain of stability becomes even larger than the measured one (cf. Fig. 1). However, our main point in Refs. [9, 11] was to establish that there exists a shape instability in the relevant R_0 and P_a range, a fact which is strongly supported by Holt and Gaitan's recent data.

In figure 7 we show how the theory of refs. [9, 11] compares to Holt and Gaitan's measurements of bubble shape oscillations in the small forcing pressure – large ambient radius regimes. Again, the agreement is reasonably good.

F. Further support for the nitrogen dissociation hypothesis

Ejection of reaction products from the bubble: A very direct proof of the chemical activity inside the bubble is the detection of reaction products expelled from it. For air bubbles we expect NO and NO_2 to be produced which then dissolve in water to form nitric acid etc. This should result in a tiny PH decrease [15, 16], which, to our knowledge, has not yet been detected. However, in a recent wonderful experiment Lepoint-Mullie et al. [20] managed to detect iodine I_2 as a reaction product coming out of a single driven bubble; the surrounding fluid contained NaI and CCl_4, the dissolved gas was air.

Numerical simulations: Also Moss et al.'s numerical simulation [26] of shock dynamics, coupled to a light emission model, supports the nitrogen dissociation hypothesis. In the simulations nitrogen bubbles are found to glow 200 times weaker than argon bubbles, in contrast to all experimental observations, in which argon and air bubbles show roughly the same light intensity. Therefore, Moss et al.'s simulations suggest that a sonoluminescing air bubble contains mostly argon.

Stable SL without degassing: An immediate consequence of our theory is that stable SBSL is possible without degassing, if only the ratio of the partial argon pressure to the ambient pressure is properly adjusted. Meanwhile such experiments have been performed both by Kondic et al. [32] and Barber et al. [2]. In figure 23 of the latter paper it is reported that SL can be observed in tap water ($p_\infty/P_0 = 1$ at

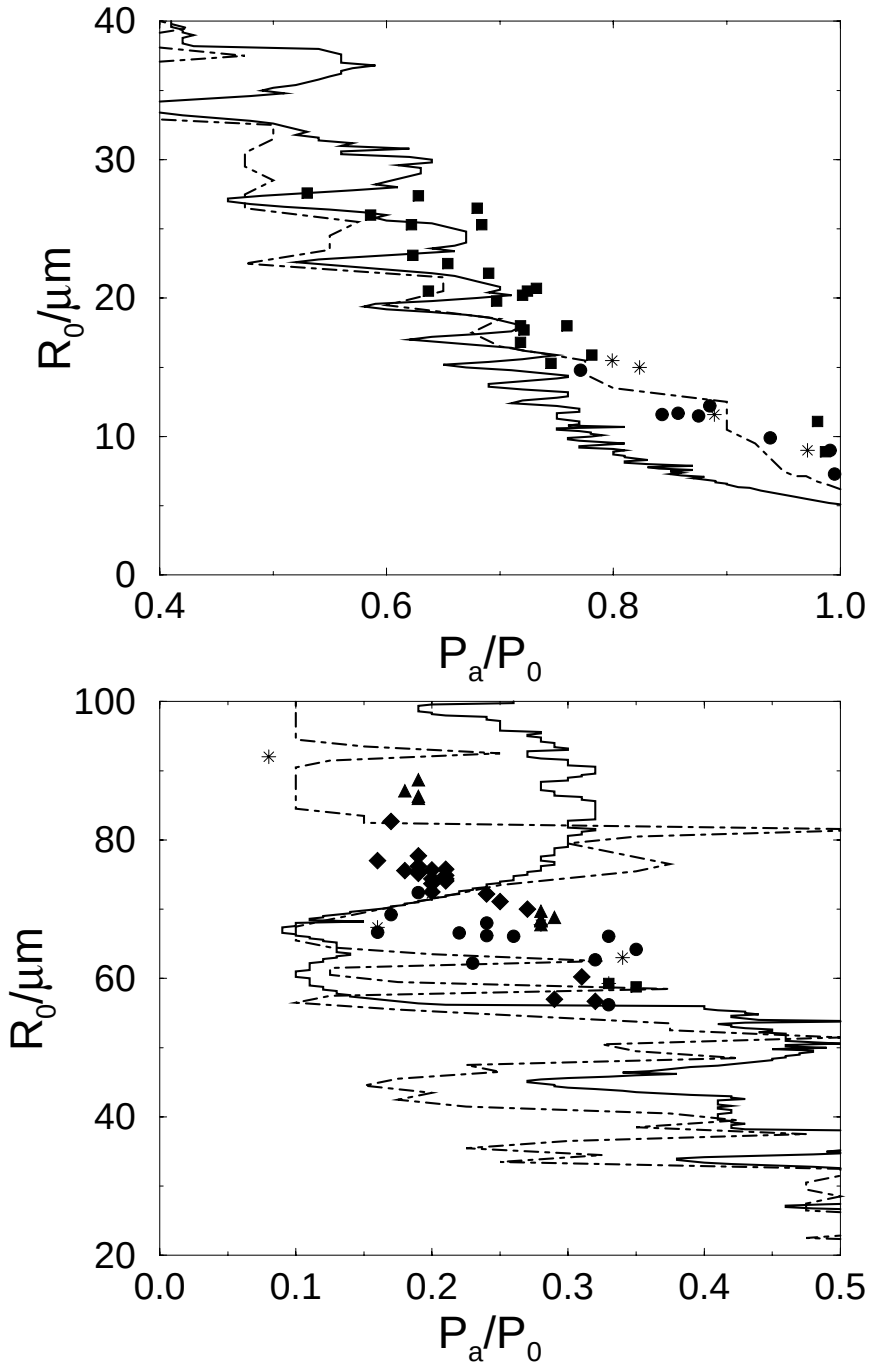

FIG. 7. Onset of shape instabilities from Holt and Gaitan's experiments [priv. communication] and from the theory of refs. [9,11] in two different non-SL regimes, $\omega/2\pi = 20.6$kHz. No data are available between these two regimes. The symbols show the measured onsets for the mode $n = 2$ (bullets), $n = 3$ (squares), $n = 4$ (diamonds), $n = 5$ (triangles), or an unknown mode (stars). The solid (dashed-dotted) line shows the theoretical onset for the n=2-mode (n=3-mode). Note that the transition of the most unstable mode from $n = 3$ to $n = 2$ is around $P_a = 0.75$atm both in experiment and theory.

ambient pressure) for $P_0 = 5$atm, i.e., $p_\infty/P_0 = 0.20$ and $p_\infty^{Ar}/P_0 = 0.002$, just as required for stable SL according to our phase diagram Fig. 3.

IV. CONCLUSION AND OUTLOOK

To summarize our findings we now explicitly answer the four questions listed in the introduction and orginally posed by Putterman's group [2]:

- Rectified diffusion, together with chemical reactions, determines the size (ambient radius) of SL bubbles. An upper limit for bubble growth is determined by shape instabilities.

- The *lower* limit in the forcing pressure P_a for SL to occur is given by a combination of shape stability, diffusive stability and the condition that the bubble wall velocity is supersonic. We stress that the experiments show excellent quantitative agreement with this calculated threshold, cf. figure 6. – The calculations (see figures 5,6, and 10 of Ref. [11]) suggest that it is the Rayleigh-Taylor shape instability which gives the *upper* limit in the forcing pressure P_a. However, we would like to stress that further instability mechanisms might exist in the large forcing pressure regime. One is the micro-jet formation as suggested by Prosperetti [33], an instability somehow related to the (short time scale) Raylor-Taylor instability [9, 11]. Another instability is caused by the Bjerknes forces becoming repulsive for large P_a. Recent calculations suggest that the Bjerknes threshold occurs around $P_a \sim 1.8$atm [34]. A consideration of the the emitted acoustic radiation from the bubble in these calculation may even shift that threshold down.

- Noble gases are essential for producing stable, bright bubbles as all molecular gases dissociate at the high temperatures achieved during bubble collapse and their reaction products dissolve in water.

- Bubbles of pure diatomic gases jitter for the same reason. They can only exist in the unstable SL domain. If they are stable as on curve B in Fig. 4a, growth by rectified diffusion and mass loss by chemical reactions are balanced. In this state, the energy focusing condition is not necessarily fulfilled, i.e., there are stable, non-sonoluminescing bubbles.

Another open question that can be rationalized using the above approach is the dependence of the sonoluminescence intensity on the temperature of the liquid: The rationalization relies on the fact that the saturated gas concentration increases with decreasing liquid temperature. Thus, according to the phase diagrams presented above, when the temperature is lowered, the pressure range where stable sonoluminescence can occur is increased. This means that at lower temperatures, it is possible

to force the bubble harder, which produces a larger light intensity. The temperature dependence of sonoluminescence can however be rationalized in other ways: for example, decreasing the temperature decreases the speed of sound of the gas which increases the coupling between the gas and the liquid [26, 27]. Published experiments have not yet distinguished between the various possibilities.

The solution of other open questions require knowledge of the energy focusing and light emission mechanisms. Compelling experimental evidence distinguishing between various theories is still lacking. The major stumbling block in our view is the current disagreement in the literature on the width of the light pulse: Original measurements showing pulse widths lower than $50ps$ have been challenged by Gompf *et. al.* [22], who measure pulse widths in the range from $100 - 300ps$. This difference is of utmost importance: Whereas the former measurements bounding the pulse width at $50ps$ [2, 23] allowed for speculation on huge energy energy focusing up to table top fusion [35], the newer measurements do not. This is because, as noted by Gompf et al., the newer measurements of the pulse width are of order the time the bubble spends in its collapsed state; this is exactly what would be expected from simple adiabatic heating of the gas. Indeed, the variation of the pulse width with experimental parameters p_∞/P_0 and P_a/P_0 observed in the Gompf et al. experiment [22] can be rationalized simply by studying the variation of the pulse width as a function of p_∞/P_0 and P_a/P_0 in the phase diagrams calculated above. Until the experimental controversy on the pulse width is resolved, it is impossible to validate adiabatic heating or other theories of energy focusing (e.g. shocks [25, 26]). If Gompf et al.'s experimental results holds up, then it seems that the explanation for single bubble sonoluminescence will be "classical bubble dynamics with a twist"–the twist coming both from the interaction of chemistry with hydrodynamic stability, and from the nonhomologous motion of the gas within the bubble.

Acknowledgments: We would like to thank G. Holt and F. Gaitan for data exchange and for allowing us to reproduce their figures. We are grateful to them and to T. Matula for various discussions. – Support for this work by the National Science Foundation Division of International Programs, and the Deutsche Forschungsgemeinschaft (DFG) under grant SBF185-D8 is gratefully acknowledged.

e-mail addresses:
brenner@math.mit.edu
hilgenfeldt@stat.physik.uni-marburg.de
lohse@stat.physik.uni-marburg.de

[1] D. F. Gaitan, Ph.D. thesis, The University of Mississippi, 1990; D. F. Gaitan, L. A. Crum, R. A. Roy, and C. C. Church, J. Acoust. Soc. Am. **91**, 3166 (1992).
[2] B. P. Barber *et al.*, Phys. Rep. **281**, 65 (1997).
[3] Lord Rayleigh, Philos. Mag. **34**, 94 (1917); M. Plesset, J. Appl. Mech. **16**, 277 (1949); J. B. Keller and M.J. Miksis, J. Acoust. Soc. Am. **68**, 628 (1980).
[4] M. Plesset and A. Prosperetti, Ann. Rev. Fluid Mech. **9**, 145 (1977).
[5] A. Prosperetti, Quart. Appl. Math. **34**, 339 (1977).
[6] R. Löfstedt, B. P. Barber, and S. J. Putterman, Phys. Fluids A **5**, 2911 (1993).
[7] M. M. Fyrillas and A. J. Szeri, J. Fluid Mech. **277**, 381 (1994).
[8] R. Löfstedt, K. Weninger, S. J. Putterman, and B. P. Barber, Phys. Rev. E **51**, 4400 (1995).
[9] M.P. Brenner, D. Lohse, and T.F. Dupont, Phys. Rev. Lett. **75**, 954 (1995).
[10] M.P. Brenner, D. Lohse, D. Oxtoby, and T.F. Dupont, Phys. Rev. Lett. **76**, 1158 (1996).
[11] S. Hilgenfeldt, D. Lohse, and M. P. Brenner, Phys. Fluids **8**, 2808 (1996).
[12] S. Hilgenfeldt, M. P. Brenner, S. Grossmann, and D. Lohse, submitted to J. Fluid Mech. (1997).
[13] C. E. Brennen, *Cavitation and Bubble Dynamics* (Oxford University Press, Oxford, 1995).
[14] M. P. Brenner, S. Hilgenfeldt, and D. Lohse, in *Nonlinear Physics of Complex Systems – Current Status and Future Trends*, edited by J. Parisi, S. C. Müller, and W. Zimmermann (Springer Lecture Notes in Physics, Berlin, 1996), p. 79.
[15] D. Lohse *et al.*, Phys. Rev. Lett. **78**, 1359 (1997).
[16] D. Lohse and S. Hilgenfeldt, J. Chem. Phys., in press (to be published November 1997).
[17] G. Holt and F. Gaitan, Phys. Rev. Lett. **77**, 3791 (1996).
[18] T. J. Matula and L. A. Crum (unpublished).
[19] J. Holzfuss, M. Rüggeberg, and A. Billo, Fortschritte der Akustik DAGA (1997).
[20] F. Lepoint-Mullie, T. Lepoint, and A. Henglein (unpublished).
[21] B. P. Barber *et al.*, Phys. Rev. Lett. **72**, 1380 (1994).
[22] B. Gompf *et al.*, Phys. Rev. Lett., in press (to be published August 1997).
[23] B. P. Barber and S. J. Putterman, Nature (London) **352**, 318 (1991).
[24] M. J. Moran *et al.*, Nucl. Instr. and Meth. in Phys. Res. B **96**, 651 (1995).
[25] P. Jarman, J. Acoust. Soc. Am. **32**, 1459 (1960); H. P. Greenspan and A. Nadim, Phys. Fluids A **5**, 1065 (1993); C. C. Wu and P. H. Roberts, Phys. Rev. Lett. **70**, 3424 (1993); W.Moss, D. Clarke, J. White, and D. Young, Phys. Fluids **6**, 2979 (1994); L. Kondic, J. I. Gersten, and C. Yuan, Phys. Rev. E **52**, 4976 (1995).
[26] W. Moss, D. Clarke, and D. Young, Science **276**, 1398 (1997).
[27] M. P. Brenner, S. Hilgenfeldt, D. Lohse, and R. Rosales, Phys. Rev. Lett. **77**, 3467 (1996).
[28] M. Plesset, J. Appl. Phys. **25**, 96 (1954).
[29] P.S. Epstein and M.S. Plesset, J. Chem. Phys. **18**, 1505 (1950).

[30] A. Eller and H. G. Flynn, J. Acoust. Soc. Am. **37**, 493 (1964).
[31] B. P. Barber, K. Weninger, R. Löfstedt, and S. J. Putterman, Phys. Rev. Lett. **74**, 5276 (1995).
[32] L. Kondic, C. Yuan, and C. K. Chan (unpublished).
[33] A. Prosperetti, J. Acoust. Soc. Am. **101**, 2003 (1997).
[34] I. Akhatov *et al.*, Phys. Rev. E **55**, 3747 (1997); T.J. Matula, S. M. Cordry, R. A. Roy, and L. A. Crum, J. Acoust. Soc. Am., in press (1997).
[35] W.Moss, D. Clarke, J. White, and D. Young, Phys. Lett. A **211**, 69 (1995).